

PACS numbers: 81.16.Nd; 81.16.Rf
DOI: 10.1070/QE2008v038n11ABEH013723

Nanosize relief: from phase masks to antireflection coatings on quartz and silicon

Yu.K. Verevkin, A.Yu. Klimov, B.A. Gribkov, V.N. Petryakov, E.V. Koposova, S.M. Olaizola

***Abstract*. By using the interference of pulsed radiation and a complete lithographic cycle, phase masks on quartz and antireflection structures on quartz and silicon are produced. The transmission of radiation through a corrugated vacuum – solid interface is calculated by solving rigorously an integral equation with the help of a computer program for parameters close to experimental parameters. The results of measurements are in good agreement with calculations. The methods developed in the paper can be used for manufacturing optical and semiconductor devices.**

Keywords: *interference of pulsed radiation, phase masks, antireflection structures, computer programs.*

1. Introduction

Nanosize periodic and quasi-periodic relieves on fused quartz are of interest for applications in various optical and electronic devices. These are first of all phase masks used for copying resonance Bragg reflectors for fibreoptic and planar devices [1 – 3], one- and two-dimensional nanoprinting stamps [4 – 6], broadband antireflection structures [7, 8], and other devices [9, 10].

Periodic phase masks are most often produced by the methods of electron-beam lithography. In this paper, we develop a simpler and more adequate method of interference lithography using a high-power pulsed XeCl laser emitting high-quality radiation. An advantage of this method is that the results of nanosize modification are weakly subjected to the influence of mechanical vibrations in the optical setup. In addition, the output energy of pulsed lasers can be increased up to a few tens of joules. This makes it possible to fabricate nanosize structures on areas of up to 1000 cm^2.

Yu.K. Verevkin, A.Yu. Klimov, B.A. Gribkov, V.N. Petryakov, E.V. Koposova Institute of Applied Physics, Russian Academy of Sciences, ul. Ul'yanova 46, 603950 Nizhnii Novgorod, Russia; e-mail: verevkin@appl.sci-nnov.ru;
S.M. Olaizola CEIT Centro de Estudios e Investigaciones Technical de Guipuzcoa, P°. Manuel Lardizábal, 15, 20.018 Donostia-San Sebastian, Spain

Received 1 August 2007; revision received 1 April 2008
Kvantovaya Elektronika **38** (11) 1078 – 1082 (2008)
Translated by M.N. Sapozhnikov

2. Estimates of a surface relief for production of phase masks and antireflection structures

Phase masks should have minimal transmission in the zero diffraction order, which should be lower than 10 %. It follows from elementary physical considerations that the minimal transmission in the zero diffraction order can be obtained at the relief depth $h \approx \lambda[2(n-1)]^{-1}$, where λ is the radiation wavelength used for copying and n is the refractive index of the phase mask material. This condition provides the intensity minimum in the zero diffraction order for a wave incident normally on a rectangular relief. This estimate is quite approximate, and a more accurate theory and more accurate measurements are required.

Antireflection structures should satisfy two conditions: the relief period d should satisfy the relation $d < \lambda_a/n$ and the relief height h should be approximately equal to $\lambda_a/4$, where λ_a is the radiation wavelength for which the antireflection coating should be fabricated. The first of these conditions is required to suppress the excitation of diffraction orders inside a medium, while the second one provides the minimal reflection of light to the zero diffraction order.)

3. Experimental setup and measurement results

We used in our experiments a 308-nm XeCl laser emitting 10 – 15-ns, 100-mJ pulses. The coherence length of laser radiation was ~ 30 cm and its divergence was nearly diffraction-limited.

A relief was produced on quartz by using a complete lithographic cycle. A mask was a two-layer structure consisting of a 50-nm-thick copper film and a 400-nm photoresist. The mask pattern was produced by irradiating the photoresist by two 30-mJ cm^{-2} beams from the XeCl laser. The two beams were obtained in a dielectric beamsplitter with the reflectance $R \sim 50$ % and were made coincident in the photoresist plane by using an optical scheme with three dielectric mirrors with $R \sim 99$ %. The mask pattern was developed on the photoresist by using a water – alkali solution, while copper was etched by the ion-beam method. Quartz was etched by the method of ion-beam reactive etching in the $CF_4 - O_2$ gas mixture flow at etching rates 30 nm min^{-1}. The etching rates of mask materials were 30 nm min^{-1} for the photoresist and 3 nm min^{-1} for copper. As a result, various relieves of depth up to 500 nm were produced on quartz.

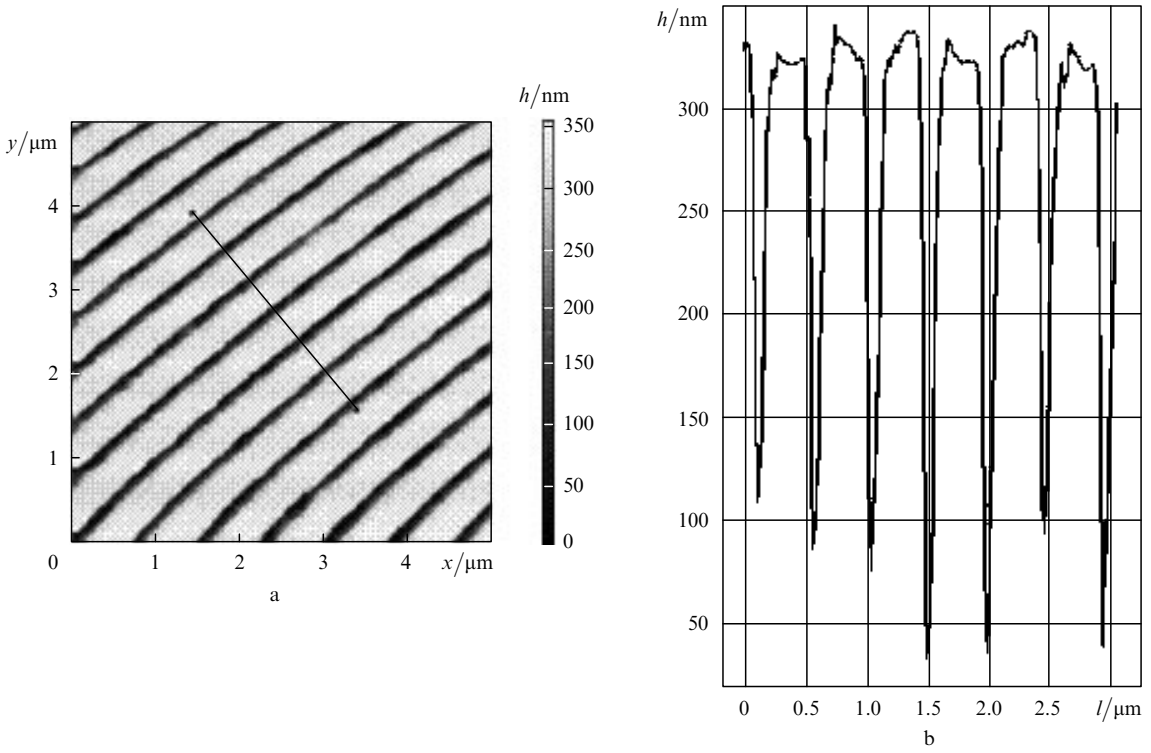

Figure 1. AFM image of a region of fused quartz (a) and its section (indicated by the straight line in Fig. 1a) (b) after the end of the total lithographic cycle; l is the coordinate along the section line.

Figure 1 shows an atomic force microscope (AFM) image of a region of fused quartz and its section (indicated by the straight line in Fig. 1a) after the end of the complete lithographic cycle. The relief period d and its mean height h can be estimated from Fig. 1 as 460 and 280 nm, respectively. Note that the minima and maxima in the relief have different widths. These parameters depend on the regimes of photoresist development and metal mask and quartz etching. The transmission coefficient of this sample in the zero diffraction order was measured with a Specord M40 (Carl Zeiss, Jena) spectrophotometer and a XeCl laser. The radiation beam diameter in both cases was ~ 5 mm and a double-beam measurement scheme was used.

Figure 2 shows the transmission spectra of quartz plates. Curve (*2*) corresponds to the transmission coefficient of a fused quartz plate with a periodic relief produced on one of its sides (the AMF image of this sample is presented in Fig. 1). The cross in Fig. 2 indicates the value of the transmission coefficient measured by using the XeCl laser. The minimal transmission coefficient in the zero diffraction order is achieved at ~ 250 nm, while antireflection properties are observed for radiation at $\lambda_a > 630$ nm. Note that this structure has an interesting feature because it can be used both as a phase mask at ~ 250 nm and as an antireflection structure for $\lambda_a > 630$ nm.

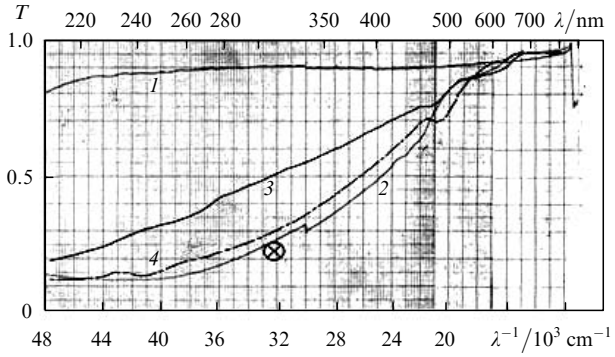

Figure 2. Experimental transmission spectra of quartz plates without a periodic relief (*1*) and with a periodic relief on one side of the plates (*2*), and theoretical transmission spectra of fused quartz plates with one corrugated boundary for $h = 280$ (*3*) and 390 nm (*4*). The cross indicates the value of the transmission coefficient measured by using the XeCl laser.

4. Calculation of characteristics of diffracted waves and comparison with the results of measurements

The dependences of the transmission of a corrugated vacuum–fused quartz interface on the ratio of the relief period to the wavelength were calculated by using a program for the numerical solution of the integral equation for the diffraction of a plane wave from a corrugated interface [11]. Calculations were performed for two relief profiles: a sinusoidal one and a relief close to the experimental relief, which was approximated by a sinusoid with a flat maximum. Figure 3 presents the half-tone transmission diagrams for these two profiles. The clearness of the diagrams is improved to simplify the determination of extremal values in them by representing the regions near the maximum and minimum transmission coefficients in diagrams by the 'inverse' colour, i.e. the region corresponding to the blackest colour is shown by a white spot (maximum), which is distinctly visible against the black background, and a black spot (minimum) shows the whitest region. Diagrams are constructed for the mean transmission

coefficient obtained for radiation with the E and H polarisations (the E polarisation corresponds to the electric field of a light wave directed along the relief lines, while the H polarisation corresponds to the magnetic field of a light wave directed along the relief lines). The refractive index of fused quartz was set equal to 1.46 in calculations, according to the reference data for the wavelength range under study. Absorption in the medium was neglected in calculations.

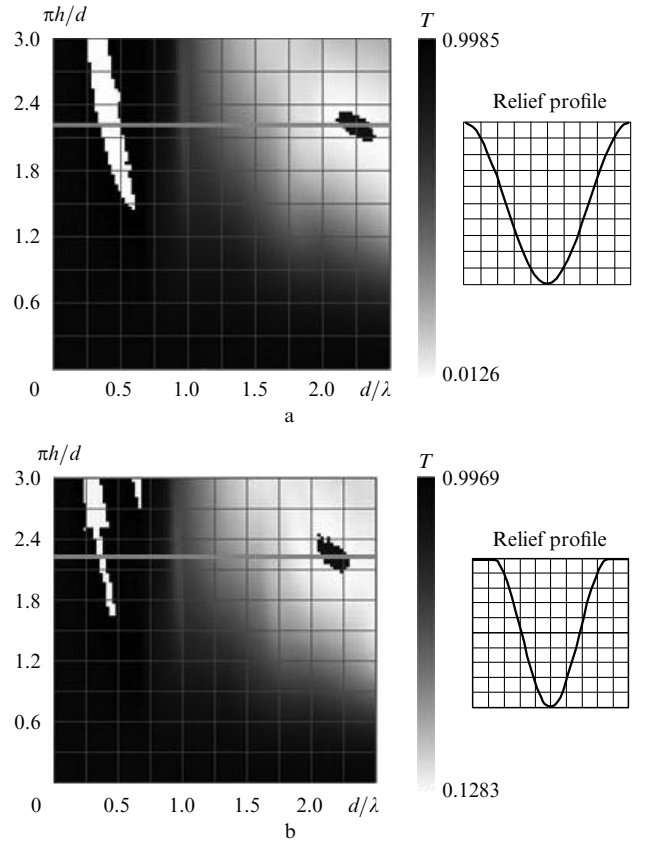

Figure 3. Theoretical half-tone diagrams of the transmission coefficient of the corrugated vacuum–fused quartz surface for the sinusoidal surface profile (a) and the surface profile close to the experimental one (b). The regions close to the maximum and minimum of the transmission coefficient are indicated by the 'inverse' colour.

Both for the sinusoidal relief and the relief close to the experimental one, the theoretical maximum of the transmission coefficient is close to unity in the extended enough region of long wavelengths (exceeding the period d) and for high relief heights h (greater than the wavelength and half the period). In this case, the transmission coefficient depends only weakly on the profile shape. The minimum of the transmission coefficient for the sinusoidal relief decreases almost to zero for $d/\lambda \sim 2.25$ and $\pi h/d \sim 2.21$, while for the experimental relief the minimum is displaced to the lower values of d/λ, being smaller than 13 %.

Figure 4 presents the dependences of the transmission coefficient on the parameter d/λ for relief heights corresponding to the minimum of the transmission coefficient (in the sections of diagrams in Fig. 3 indicated by grey straight lines). For a real physical structure having a certain relief period ($d = 460$ nm) and a certain height (the ratio $\pi h/d \sim 2.21$ for this period corresponds to the height $h \sim 323$ nm),

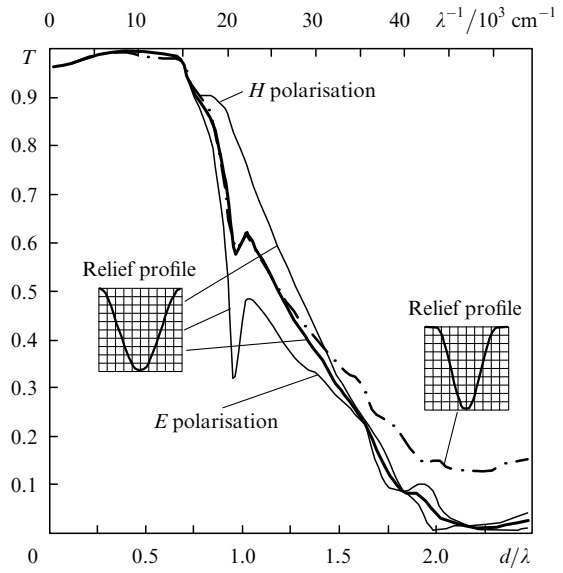

Figure 4. Dependences of the transmission coefficient of the corrugated vacuum–fused quartz interface on the ratio of the relief period to the wavelength calculated for relief heights corresponding to the minimum of the transmission coefficient (in diagram sections indicated by grey straight lines in Fig. 3) for the sinusoidal relief profile and the surface profile close to the experimental one and different polarisations of probe radiation.

these curves are the dependences of the transmission coefficient on the inverse wavelength (or the wave number).

The solid thick curve is constructed for the sinusoidal relief, while the dot-and-dash thick curve corresponds to the nearly experimental relief. These curves are the dependences of the averaged transmission coefficient for radiations of the E and H polarisations, i.e. for nonpolarised radiation (which is used, as a rule, in spectrophotometers). Thin curves are the dependences for the E and H polarisations constructed for the sinusoidal relief. The difference in the behaviour of these curves is significant near the wavelength λ_1^* equal to the period d. This wavelength is the boundary (maximal) wavelength of the region of existence of the first diffraction beam in vacuum (it was assumed that the refractive index of the environment is $n = 1$). In the case of the E polarisation, a characteristic narrow hole exists at λ_1^*, while for the H polarisation, a flat shoulder is observed. Note that the averaged (solid thick) curve also exhibits the characteristic (although smoothed) hole at λ_1^*.

There also exists another point, which is important for analysis of experimental data. This is the point of a sharp break in the curves in the wavelength region for $\lambda_2^* = dn$. The wavelength λ_2^* is the boundary (maximal) wavelength of the domain of existence of the first diffraction order in the medium. The behaviour of all the curves near λ_2^* in Fig. 4 is identical and is independent of the relief shape and polarisation. In passing from the long-wavelength region, where the transmission coefficient is close to unity, to the shorter-wavelength region, the transmission coefficient drastically decreases. The real refractive index of a sample can be determined from the position of this point, if the structure period is known accurately enough.

Figure 2 shows the calculated transmission spectra [curves (*3*) and (*4*)] of a fused quartz plate with one corrugated boundary. They were obtained by solving the

integral equation for one corrugated boundary taking into account the additional reflection of light from the flat boundary and using the relief profile close to the experimental one (Fig. 1). The refractive index $n = 1.46$ was determined from the corresponding experimental curve in Fig. 2 for $\lambda_2^* = dn \sim 650$ nm and $d = 460$ nm. The behaviour of this curve suggests that the H-polarised radiation dominates because a narrow hole at the point $\lambda = d$ is absent, while this hole is observed in the cases of the E-polarised and nonpolarised radiations. More careful estimates gave the assumed ratio of the fractions of the E- and H-polarised radiations equal to 1 : 4. The curves were constructed for two relief heights $h = 280$ and 390 nm. Curve (*3*) coincides with experimental curve (*2*) only in the long-wavelength and intermediate regions, while in the shorter-wavelength region it runs above curve (*3*). Curve (*4*) better coincides with the experimental curve in the short-wavelength region, while the agreement with the experimental curve in the intermediate region between the long-wavelength and short-wavelength regions is worse. Such a partial coincidence suggests that the model of the relief profile used in calculations is too rough and is also caused by the influence of the scatter in the heights and shapes of a real manufactured structure.

5. Periodic structures on silicon and measurements of their parameters

Silicon can be efficiently used in optical devices operating in the IR region. A periodic nanosize relief produced on the silicon surface can be used to fabricate photonic crystals, multiplexers and antireflection structures [12–14]. We describe below the production of an antireflection structure.

Figure 5 presents the AFM image of the surface of silicon single crystals with a periodic relief. This structure with the characteristic diameter above 6 mm was fabricated by using methods described above for quartz. One can see from Fig. 5b that the relief period is 460–480 nm and its depth varies from 350 to 370 nm. Based on the estimates made above, we can expect that such a structure will reveal antireflection properties for radiation at $\lambda > 1.5$ μm.

Figure 6 shows the IR transmission spectra of silicon plates recorded with a SF-20 (LOMO) spectrophotometer and theoretical spectra obtained by solving the integral equation taking into account transmission through a flat boundary. The plates had different thicknesses and different relief heights. Curve (*1*) has wavelength marks separated by the 10-nm interval. Curves (*2–4*) demonstrate a considerable increase in the transmission coefficient of a plate with the relief for $\lambda > 1.5$ μm, in accordance with simple estimates. A more detailed analysis of the experimental curves gives the wavelength $\lambda_2^* = dn$ (~ 1.530 μm), which, taking into account the estimate of the period $d = 466$ nm from Fig. 5, allows us to estimate the refractive index of the sample as $n \simeq 3.28$. Curves (*5*) and (*6*) are theoretically calculated for this refractive index and the relief close to that presented in Fig. 5. The period of this relief was described by a sinusoid with a flat maximum of width equal to 1/5 of the relief period. The calculation was performed for two depths of 350 and 400 nm. The polarisation of probe radiation in experiments was unknown and it was selected for theoretical calculations to provide the best coincidence between the slopes of theoretical and experimental curves.

Our study has shown that the E polarisation dominates in probe radiation (the ratio of the E and H polarisations was 5 : 1). Such a choice is reasonable and possible, which

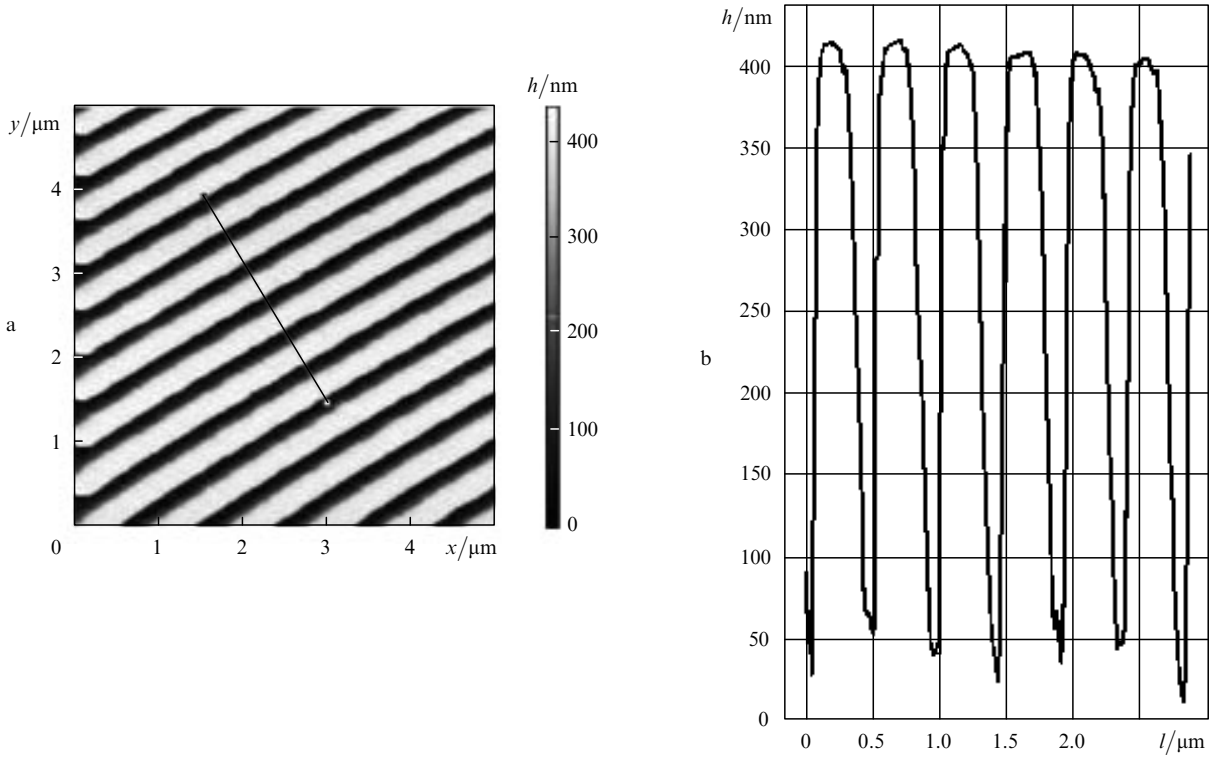

Figure 5. AFM image of the surface of a silicon single crystal (a) and its section (indicated by the straight line in Fig. 5a) after the end of the total lithographic cycle; l is the coordinate along the section line.

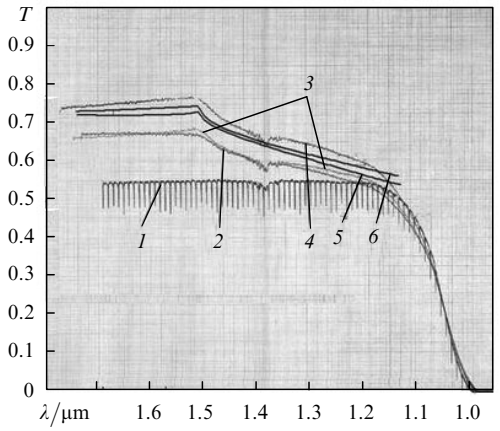

Figure 6. Experimental transmission spectra of a plane–parallel silicon plate (*1*) and silicon plates with a periodic relief on one surface (*2–4*) and transmission spectra calculated for the sinusoidal relief with $h = 350$ (*5*) and 400 nm (*6*).

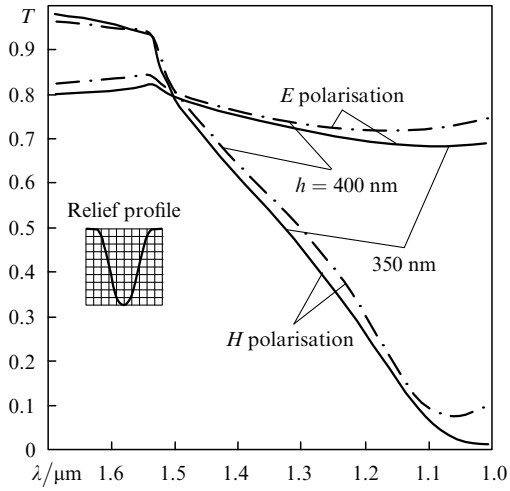

Figure 7. Transmission spectra of the corrugated silicon surface with the relief profile close to that presented in Fig. 5 calculated for different relief heights and different polarisations of radiation.

follows from the qualitatively different behaviour of the curves calculated separately for each polarisation, as is demonstrated in Fig. 7. The difference between the curves for different polarisations is considerably greater than that between the curves for different relief heights in the height range under study. The experimental transmission coefficient differs from the theoretical one (equal to 100 % in the ideal case) because the second surface of silicon had no relief. Absorption in silicon was neglected in calculations because antireflection structures are mainly of interest in its transparency range.

Theoretical curves in Fig. 6 are constructed only for wavelengths $\lambda > 1.15$ μm for which the experimental transmission coefficient of a plane–parallel plate is constant. Note that such antireflection coatings can be used in solar elements [15] and for the production of periodically arranged germanium isles on silicon [16, 17].

6. Conclusions

By using pulsed interference lithography, we have developed the technology for production of submicron relieves to fabricate phase masks and antireflection structures. A comparison of the results of measurements and calculations has indicated the possible direction in the optimization of such structures.

Acknowledgements. This paper was partially supported by Grant 'Development of Lithography of Materials Using Laser Beam Interference' EC FP-6 IST-4 No. 027976 and the program 'Nonlinear Optics of Unique Laser Systems' of the Department of Physical Sciences, RAS.

References

1. Dragomir N.M., Rollinson C., Wade S.A. *Opt. Lett.*, **28** (10), 789 (2003).
2. Park D., Kim M. *Opt. Lett.*, **29** (16), 1849 (2004).
3. Haro-Poniatowski E., Fort E., Lacharme J.P., Ricolleau C. *Appl. Phys. Lett.*, **87**, 143103 (2005).
4. Guo L.J. *J. Phys. D: Appl. Phys.*, **37**, R123 (2004).
5. Pisignano D., Maruccio G., Mele E. *Appl. Phys. Lett.*, **87**, 123109 (2005).
6. Heon Lee, Hong S., Yang K. *Appl. Phys. Lett.*, **88**, 143112 (2006).
7. Kanamori Y., Sasaki M., Hane K. *Opt. Lett.*, **24** (20), 1422 (1999).
8. Kintaka K., Nishii J., Mazutani A., Kikuta H., Nakano H. *Opt. Lett.*, **26** (21), 1642 (2001).
9. Rastei M.V., Meckenstock R., Bucher J.P., Devaux E., Ebbessen Th. *Appl. Phys. Lett.*, **85** (11), 2050 (2004).
10. Kim D. *Appl. Opt.*, **44** (16), 3213 (2005).
11. Vlasov S.N., Koposova E.V. *Izv. Vyssh. Uchebn. Zaved., Ser. Radiofiz.*, **46**, 482 (2003).
12. Brundrett D., Gaylord T., Glytsis E. *Appl. Opt.*, **37** (13), 2534 (1998).
13. Xu Y., Sun H., Ye J., Matssuo S., Misawa H. *J. Opt. Soc. Am. B*, **18** (8), 1084 (2001).
14. Wang S., Zhou C., Zhang Y., Ru H. *Appl. Opt.*, **45** (12), 2567 (2006).
15. Zeng L., Hong Y., Liu J., Feng N., Duan X., Kimerling L., Alamariu B. *Appl. Phys. Lett.*, **89**, 111111 (2006).
16. Guise P., Yates J., Levy J., Ahner J., Vaithynathan V., Schlom D. *Appl. Phys. Lett.*, **87**, 171902 (2005).
17. Zhong Z., Katsaros G., Stoffel M., Costantini G., Kern K., Schidt G., Jin-Phillipp N., Bauer G. *Appl. Phys. Lett.*, **87**, 263102 (2005).